Anchoring a Liquid Crystal Molecule on a Single-Walled Carbon Nanotube

Kyung Ah Park,[†] Seung Mi Lee,[‡] Seung Hee Lee,[§] and Young Hee Lee*,[†]

Department of Physics, Center for Nanotubes and Nanostructured Composites, Sungkyunkwan University Advanced Institute of NanoTechnology, Sungkyunkwan University, Suwon 440-746, Republic of Korea, BK-21 Polymer BIN Fusion Research Team, Research Center of Industrial Technology, Chonbuk National University, Chonju, Chonbuk 560-756, Korea, and Korea Research Institute of Standards and Science (KRISS), Yuseung-Gu, Daejeon 305-600, Korea

Received: September 14, 2006; In Final Form: October 31, 2006

The atomic and electronic structures of the tri-fluorophenyl2 (TFP2) liquid crystal (LC) molecule anchored on a carbon nanotube (CNT) wall were investigated by using density functional calculations. The TFP2 LC molecule was anchored helically to the CNT wall to enhance $\pi-\pi$ stacking by maximizing the hexagon−hexagon interactions between two species. The anchoring was further strengthened with a binding energy of nearly −2.0 eV by electrostatic energy due to a considerable amount of charge transfer from LC molecule to the CNT. These charges were distributed asymmetrically on the CNT due to the anchoring of asymmetric LC molecule, which induced a permanent dipole moment on the CNT. This plays an important role for electro-optical responses of CNTs in the LC cell. Our theoretical study can explain the recent experimental report for the various dynamical motions of CNT in the LC cell under an external electric field.

Introduction

Since the discovery of carbon nanotubes (CNTs),[1−3] extensive studies of the unique physical and chemical properties of CNTs and their diverse applications have been reported.[4−6] The superb electrical conductivity and high mechanical strength of CNTs have opened potential application areas in composites with polymers, ceramics, and metals.[7−9] For instance, the limitations of conductivity and mechanical strength in polymers could be overcome by adding a minute quantity of CNTs into polymers. Polymers have been known to wrap the CNTs to increase the interaction.[10] In general, the characteristics of composites are strongly governed by the interactive nature between the CNT and host material. To strengthen the binding between CNTs and host materials, serious functionalization steps for CNTs are often required, mostly damaging CNT walls.

Recently, CNTs have been introduced into the liquid crystal (LC) cell. Although LC displays are commonly available in the market, the limitations still exist in the dynamical response of the LC cell, which strongly relies on the material properties. It has been reported that a minute addition of carbon nanosolids such as C_{60} and mutiwalled CNTs dispersed in a twisted nematic LC affects the electro-optical properties of the cell. Among them are the threshold voltage, response time, and residual DC.[11−16] One interesting feature is that the long CNTs can be well-aligned in a nematic LC medium in the absence of an external field. Furthermore, the CNTs can orient with an external field above some critical field strength.[17−20] In spite of numerous experimental observations, the percolation limit on the quantity of CNTs that can be dispersed in LC medium is still subject to debate. The degree of dispersion is strongly dependent on the dispersion process such as solvent types and sonication. Yet, the binding nature between the CNT and LC molecule is another important ingredient not only in determining the percolation limit from the material point of view but also in understanding the alignment of CNTs in LC medium and the dynamical response of CNTs under an external field. To our knowledge, no systematic report on the interactive nature between the CNT and LC molecule is currently available.

In this article, we report on our thorough investigation of the interactive nature between a CNT and LC molecule by using density functional calculations. By choosing a conventional fluorinated LC molecule, the stable geometries of LC molecules anchored on the CNT wall were systematically searched in our approach. The atomic structures, binding energy, charge transfer, and electronic structures of the stable geometries were evaluated in detail. This enabled us to estimate a permanent dipole moment of the CNT that may explain the dynamical responses of CNTs in the LC medium.

Theoretical Methods

Our total energy calculations and corresponding structure optimizations of the most stable geometries were based on the density functional formalism within the local density approximation (LDA) and the generalized gradient approximation (GGA) as implemented in DMol3 code.[21] The exchange correlation energy in the LDA was parametrized by Perdew and Wang's scheme,[22] and Becke's corrected exchange functionals were adopted in the GGA.[23] All-electron Kohn−Sham wave functions were expanded in a local atomic orbital basis set with each basis function defined numerically on an atomic-centered spherical polar mesh. We used a double numeric polarized basis set. The most complete set is available in DMol^3 code. In this basis set, the 2s and 2p carbon, fluorine, and oxygen orbitals were represented by two wave functions each, and 3d (2p)-type wave functions on each of the carbon, fluorine, and oxygen (hydrogen) atoms were used to describe the polarization. No frozen core approximation was used throughout the calculations. For accurate binding energy calculations, GGA calculations were

* Corresponding author. E-mail: leeyoung@skku.edu.
[†] Sungkyunkwan University.
[‡] KRISS.
[§] Chonbuk National University.

10.1021/jp0659960 CCC: $37.00
Published on Web 01/05/2007

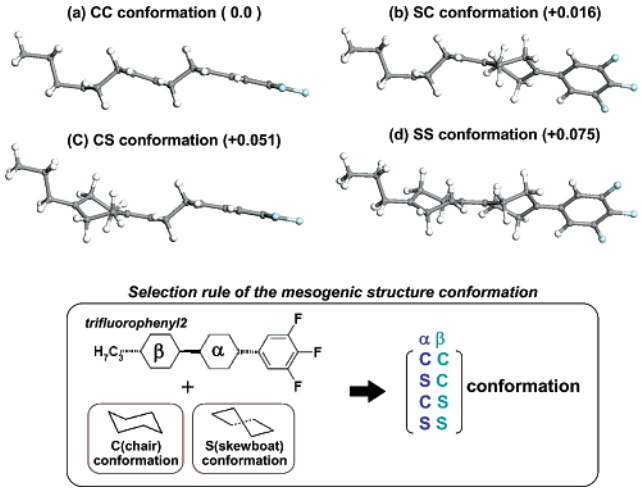

Figure 1. Various atomic conformation structures of the LC molecule. The schematic in the box shows the conformation selection rule for the two cyclohexane ring structures on the TFP2 LC. (a) CC: chair−chair conformation, (b) SC: skewboat−chair conformation, (c) CS: chair−skewboat conformation, and (d) SS: skewboat−skewboat conformation. The values in this figure indicate the relative binding energy with respect to the CC conformation in electronvolt units.

performed after geometrical optimization by the LDA. The forces on each atom to be converged during each relaxation were less than 0.002 atomic units with a displacement convergence of 0.005 Å. The binding or adsorption energy (E_{ad}) of the LC molecule on the CNT wall was defined as $E_{ad} = E_t(\text{CNT} + \text{LC}) - E_t(\text{CNT}) - E_t(\text{LC})$, where E_t is the total energy of a given system.

We chose a typical superfluorinated LC molecule, 2,3,4-trifluorophenyl2 (TFP2), as a model calculation; TFP2 is a mostly available material for commercial displays. This molecule was composed of a hexagonal head part with three fluorine atoms, two cyclohexane rings as mesogenic group, and an alkyl chain tail part. The head part contained polar terminal group or polar lateral group and mainly determined the dielectric anisotropy ($\Delta\epsilon$) of the LC molecule. We chose a (5,5) armchair CNT with the CNT length of 14 layers with 17 Å long along the tube axis. This was presumably short compared to the experimentally used one but at least longer than the LC length (15 Å) such that the interaction between the CNT and LC molecule was fully incorporated in the model calculation. Since the CNTs were usually functionalized by hydroxyl and/or carboxyl groups during the sample treatment,[24] we considered three cases of CNTs: open nanotube, hydrogen-, and oxygen-terminated nanotubes. We used these three cases to emulate the functionalized CNTs. These situations were similar to those functionalized defects at the sidewalls.

Results and Discussion

A. The Stable Geometry of the TFP2 LC Molecule. We first searched for the stable TFP2 geometry from the chemical structure. The TFP2 molecule had three fluorine atoms at the head group. The fluorine atoms (−0.312 e/atom) in the head group were mostly negatively charged. The charges were mostly extracted from hydrogen atoms (+0.18 e/atom) in the tail group. This was confirmed from the Mulliken charge population. This large charge transfer leads to the creation of a high dielectric constant. Two types of conformational combinations of chair type (C) and skewboat type (S) existed between two cyclohexane rings in the mesogenic group, as shown in the box of Figure 1. We denoted the two cyclohexane rings as α and β from the head group in Figure 1. Here, both rings were varied with a chair type and a skewboat type, as can be seen in Figure 1. We marked the chair−chair, chair−skewboat, and skewboat−skewboat conformations as CC, CS, and SS conformations, respectively. The total energies were calculated after the geometries were fully relaxed. The most stable geometry for the TFP2 was the chair−chair conformation as depicted in Figure 1a. It is well-known that the chair-type conformation is more stable than the skewboat type in a cyclohexane ring. This is because the bonding angle of the chair type is 111°. Thus, it has a minimum angle strain and torsional strain. This chair−chair geometry was used in the rest of our calculations to study the interaction between the CNT and LC molecule.

B. Interaction between the TFP2 LC Molecules. In this section, we describe the interaction between two TFP2 molecules. Figure 2 shows the interaction between these two molecules parallel to each other, as denoted for the head−head (H−H) type and the asymmetric head−head (AH−H) type, and antiparallel for the head−tail (H−T) type. The H−T type gave consistently stronger binding energy than the other two types, independent of the calculation methods and basis sets, favoring the antisymmetric H−T interaction. This explains why the nematic LC medium does not possess a permanent dipole moment despite the fact that the individual LC molecule has a permanent dipole moment.[25]

The distance between two TFP2 molecules is depicted in the Figure 2. The shortest distance between two LC molecules was about 4 Å longer than the general van der Waals interaction distance. Figure 2d,e presents the binding energy of two TFP2 molecules. This binding energy was dependent on the basis set and types of correlation energy. Independent of all these variations in the parameters, the H−T type was the most stable geometry. Because of electron charge transfer, the electrostatic interaction was dominant over van der Waals interaction. Hence, the H−T was more favorable. A more accurate GGA calculation suggested that the interaction energy may be a few meV or so. More accurate calculations with large basis sets were required to have an accurate binding energy. This reflected again the low vaporization temperature of a typical LC medium.

C. Interaction between the TFP2 LC Molecule and CNT. Figure 3 presents three types of nanotubes: an open nanotube, hydrogen-, and oxygen-terminated nanotube. In addition to representing the functionalized nanotubes, the termination of dangling bonds provided less strain to the carbon atoms near the edge, making them ideal structures. It also enhanced the computational speed by fast convergence in solving the self-consistent Kohn−Sham equation. Comparison of these three structures informed us about the interaction of the LC molecule with the functionalized nanotubes. We also defined an anchoring site of the TFP2 molecule on the CNT surface, as shown in Figure 3d. The "edge site" overlapped the outmost hexagonal ring of the CNT with that of the head group in the TFP2 molecule. The "inner site" and the "third site" refer to the second and third hexagonal ring from the CNT edge coinciding with that of the TFP2 head group. The top view of the anchored TFP2 on the "edge site" of the CNT surface was also illustrated in Figure 3d. Figure 4 presents the top and side views of the most stable geometries for different functional groups. The head group interacted with the CNT wall with the closest separation distance of nearly 3 Å, as listed in Table 1. This was independent of the functional groups. We note that the interaction was strengthened by the $\pi-\pi$ stacking among hexagonal rings in the head part of the LC molecule and those of the CNT wall. This is illustrated in Figure 3d. This explains the experimental

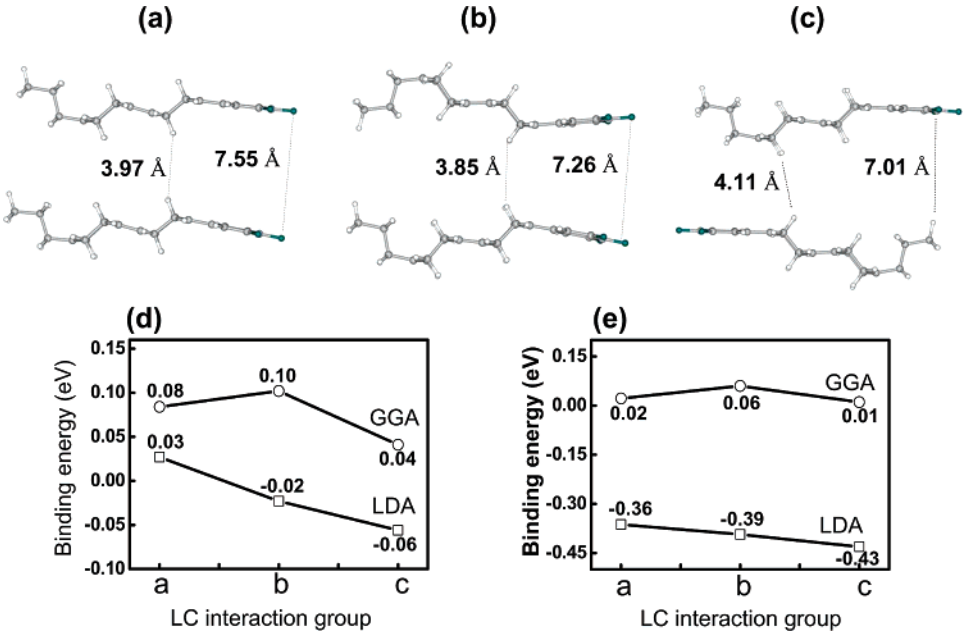

Figure 2. Interaction groups of two LC molecules defined by facing with (a) head−head (H−H), (b) asymmetric head−head (AH-H), and (c) head-tail (H−T). The calculated binding energies by the GGA and the LDA methods depend on the numerical basis sets (d) double numerical plus d-functions (DND) and (e) double numerical plus polarization (DNP). The DNP basis sets provide higher accuracy especially for the hydrogen bonding than the DND basis sets.

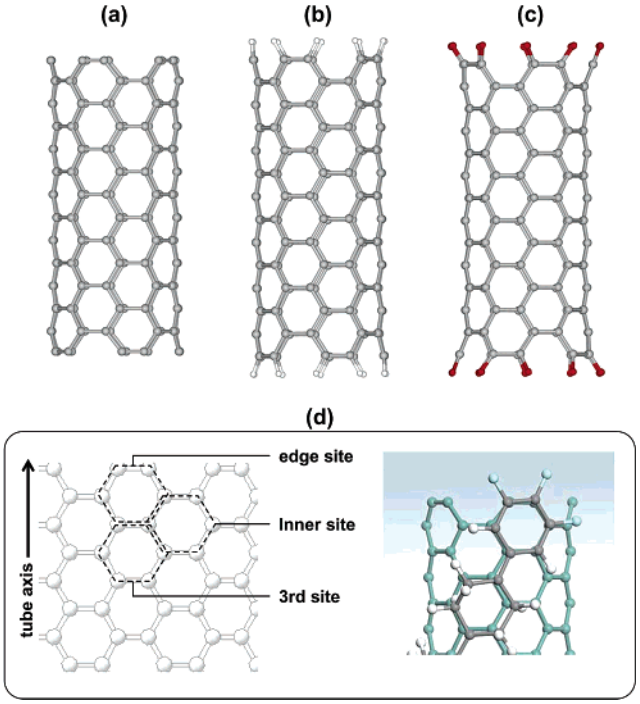

Figure 3. CNT geometries for (a) open (5,5) CNT, (b) hydrogen-terminated (5,5) CNT, and (c) oxygen-terminated (5,5) CNT. (d) The schematic top view for different LC positions from the proximate edge is also shown and the real top view of the $\pi-\pi$ stacked LC on the CNT wall.

observations that the ring-type molecule was dominated by $\pi-\pi$ stacking with the CNT wall.[26] The closest distance between the mesogenic group of the LC molecule and CNT was nearly 2 Å. The hydrogen atoms in the mesogenic group were partially positively charged, and the closest carbon atoms in the CNT backbone were partially negatively charged. This charge localization induced the hydrogen-bonding interaction between the LC molecule and CNT. On the other hand, the tail groups were strongly repelled from the CNT wall with a large separation distance of more than 5 Å. The amount of charge transfer was calculated by summing all the atoms in the LC molecule, respectively. The largest charge transfer (−0.73 e) was observed in the oxygen-terminated CNTs compared to the other types. This was ascribed to a large electronegativity of the oxygen atom compared to that of a hydrogen atom. Even in the case of open edge interaction, some charges were still transferred to the CNT. One may conjecture which interaction is dominant in Table 1. The interaction energy was roughly proportional to the amount of charge transfers among different edges, independent of the basis sets. This ensures that the hydrogen bonding prevails in the interaction. Another point to note is the position of the LC molecule. In the case of the open edge, the edge was the favorable site, whereas in the case of the functionalized edges, the inner sites were more favorable sites. Furthermore, the energy difference between inner and edge sites was not so appreciable. This suggests that the energetic is governed by the charge transfer between two molecules, not by the relative position of the LC molecule to the edge site. As a consequence, the separation distances between F, H, and O in LC molecules and carbon atoms in CNT were shorter than the typical van der Waals interaction distance of 3.4 Å, as listed in Table 1. Because of this, the binding energy was much stronger than van der Waals interaction and therefore describable in LDA limit. This resulted in a large binding energy of −2.02 eV for an oxygen-terminated one. Thus, the relevance to the real experiment is still valid for energetics, separation distances, and charge transfer. One thing to note is that the long axis of the LC molecule was anchored parallel to the tube axis. Furthermore, the binding energy between LC molecule and CNT was about −2 eV, much stronger than the physisorption energy (∼meV). This explains how the gigantic CNTs can be well-aligned in the LC medium which was observed experimentally.[17,18]

D. Charge Distribution. Because of the net charges that were present on the CNT wall, we next calculated the charge distribution in the CNT. Figure 5 presents the top and side views of the charge distribution of each orbital for the oxygen-terminated CNT. Figure 5a clearly indicates that most charges

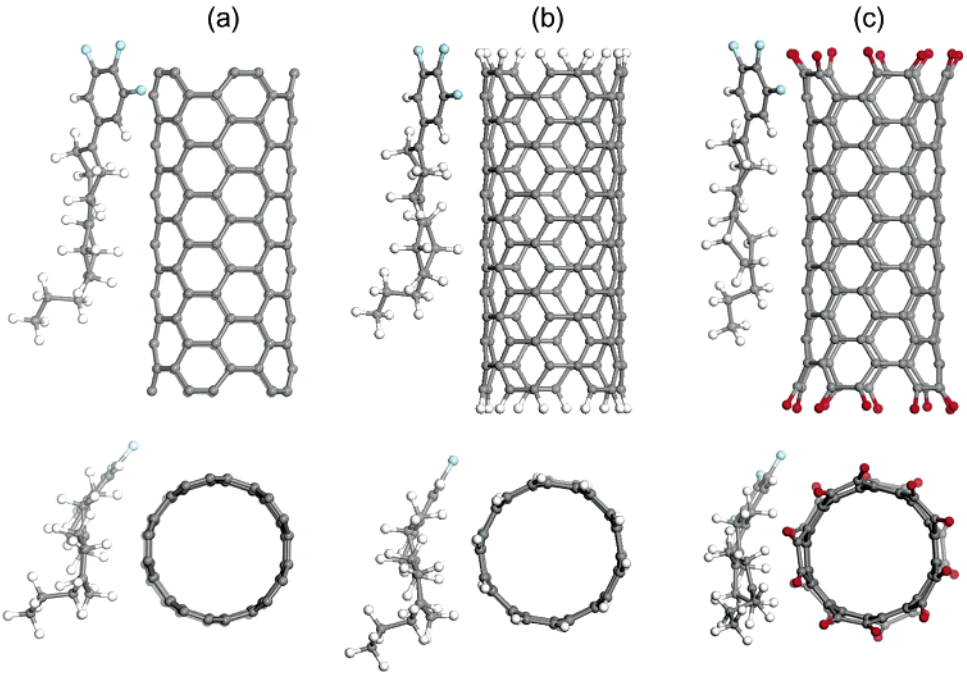

Figure 4. Side and top views of the LC molecule anchored on the edge site of (a) the bare CNT, (b) the H−CNT, and (c) the O−CNT.

TABLE 1: Various Geometric and Energetic Parameters Determined from the LDA for Each of the LC−CNT Structures[a]

	LC−CNT		LC−HCNT		LC−OCNT	
	edge	inner	edge	inner	edge	inner
bond length (Å)						
C−C	3.191	3.046	3.109	3.085	3.194	3.325
F−C	3.336	3.326	3.154	3.161	3.218	3.486
F−H(O)	*	*	2.979	2.855	2.990	2.920
H_1–C	2.226	2.283	2.258	2.214	2.143	2.150
H_2–C	2.251	2.347	2.426	2.616	2.563	2.244
E_{B-DND} (eV)	−1.27	−1.20	−1.13	−1.26	−1.77	−1.83
E_{B-DNP} (eV)	−1.46	−1.39	−1.33	−1.45	−1.96	−2.02
Δe	−0.45	−0.43	−0.26	−0.23	−0.74	−0.73
μ(D)	1.06	2.35	2.15	3.01	−2.95	0.08

[a] C−C: The closest distance between C-atom@LC and edge C-atom@CNT. F−C: The closest distance between F-atom@LC and edge C-atom@CNT. F−H(O): The closest distance between F-atom@LC and H-atom@CNT or O-atom@CNT. H_1–C(H_2–C): The closest distance between H-atom@LC and C-atom@CNT. $E_{B-DND,DNP}$: The binding energy of the LC molecule on the CNT depending on the basis set. Δe: The charge transfer from the LC molecule to the CNT. μ: The permanent dipole moment of the CNT induced by the charge transfer with respect to the center of mass.

of the highest occupied molecular orbital (HOMO) in the LC molecule were drained to the HOMO in the CNT. Although the LC molecule was located at one edge of the CNT, the HOMO was highly symmetric along the CNT axis and circumferential direction. The second and third HOMOs in the CNT became asymmetric. This led to a permanent dipole moment in the CNTs. The sparse existence of the second and third HOMO charges in the LC molecule indicated that most bonding orbitals were located in the deep energy levels. On the other hand, the lowest unoccupied molecular orbital (LUMO) charges were mostly located in the head group and the cyclohexane group and the second LUMO in the tail group, as shown in Figure 5d,e. The LUMO in the pure CNT, prior to the anchoring of LC molecule, was completely symmetric along the circumferential direction. This was filled by accepting charges from the LC molecule. The third LUMO charges were mostly located at atoms of both edges. Although our calculations

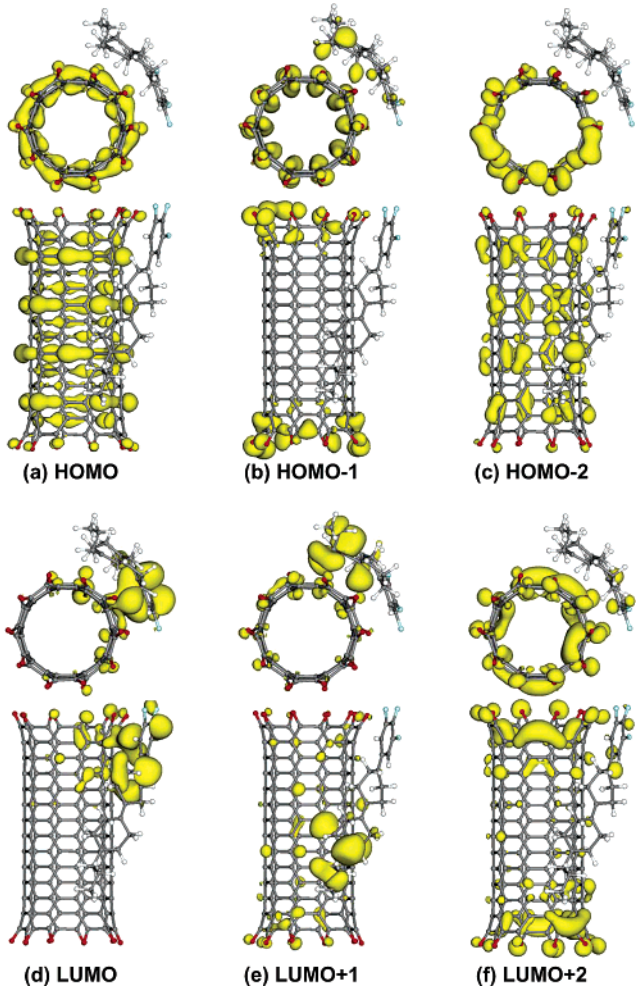

Figure 5. Charge distribution of three energy levels (occupied and unoccupied) from the Fermi level for the LC molecule anchored on the O−CNT.

were limited by the short CNT length with symmetric functionalization at both edges, this provided some intuitive pictures for the formation of a permanent dipole moment. In a real

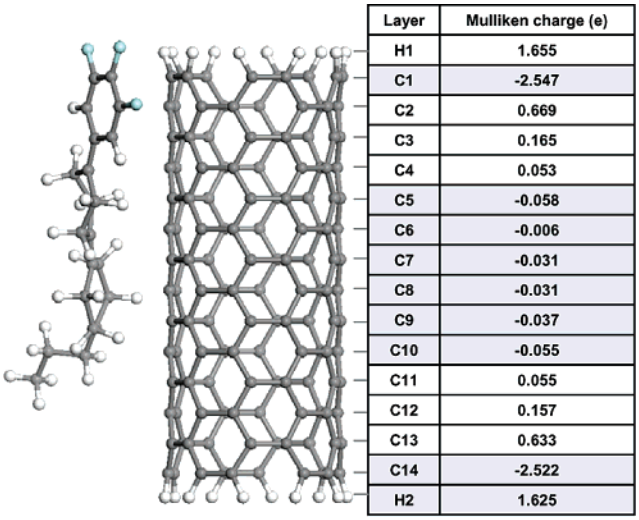

Layer	Mulliken charge (e)
H1	1.655
C1	-2.547
C2	0.669
C3	0.165
C4	0.053
C5	-0.058
C6	-0.006
C7	-0.031
C8	-0.031
C9	-0.037
C10	-0.055
C11	0.055
C12	0.157
C13	0.633
C14	-2.522
H2	1.625

Figure 6. Mulliken charge distribution on each layer of the H−CNT.

situation, the tube diameters of the single-walled CNTs were usually in the range of 1−2 nm with a length of a few micrometers. The dispersion of the CNTs in LC medium resulted in anchoring of several LC molecules along both the circumferential directions and the tube axis. The induced charge distribution in the CNTs was inevitably asymmetric, therefore producing net charges in the CNT and the permanent dipole moment. The magnitude of the dipole moment will be huge because of the long CNTs.

We next calculated the permanent dipole moment of the CNT. The Mulliken charge populations of each layer from the hydrogen-terminated CNT are shown in Figure 6. The hydrogen atoms at the edge lost charges, whereas the carbon atoms at the edge of the CNT mostly accepted charges. Some small charges were also accumulated in the carbons atoms at the center of the CNT because of the positively charged hydrogen atoms located in the cyclohexane group. The dipole moment was calculated using these charge distributions with the center of mass located at the middle of the tube. This value was the largest among the types of CNTs, as shown in Table 1. Despite a large amount of charge transfer in the case of the oxygen-terminated CNT, the charge distribution became more symmetric compared to the others, thus giving the small dipole moment. In particular, the dipole moment became negative in the case of the edge site anchoring on the oxygen-terminated CNT. This was attributed to the antisymmetric charge accumulation along the tube axis. In real experiments, the CNT lengths were typically longer than a few hundred nanometers, which resulted in a larger permanent dipole moment than that of the simulated CNT because the dipole moment is linearly proportional to the CNT length.[19,20] This large permanent dipole moment can be easily rotated at particularly high external voltage. The presence of a permanent dipole moment in the CNT resulting from the charge transfer from LC molecule can explain the simple translational motion of CNT under dc bias and its dynamical motion at ac bias with a critical field strength, which was experimentally observed.[19,20]

Conclusions

In this work, we searched for stable geometries of an LC molecule anchored on the CNT wall by using DFT. The chair−chair conformation was found to be the most stable geometry for the TFP2 LC molecule. The $\pi-\pi$ stacking between the head group in the LC molecule and on the CNT wall led to anchoring of the LC molecule on the CNT wall, whereas the tail group was repelled from the CNT wall. The binding energy of the LC molecule on the CNT wall was about −2 eV, stronger than the typical van der Waals interaction. This strong binding originated from the electrostatic energy by a significant amount of charge transfer from the LC molecule to the CNT. Further calculations of the permanent dipole moment of the CNT could explain the dynamical motion of CNTs under various external fields.

Acknowledgment. This work was supported by the KRF Grant funded by the Korean Government (MOEHRD) (KRF-2005-201-C00012), in part by the KOSEF through CNNC at SKKU (Y.H.L.), and in part by Grant No. R01-2004-000-10014-0 from the Basic Research program of the KOSEF (S.H.L.).

References and Notes

(1) Dresselhaus, M. S.; Dresselhaus, G.; Saito, R. *Phys. Rev. B* **1992**, *45*, 6234.
(2) Iijima, S. *Nature (London*) **1991**, *354*, 56.
(3) Bockrath, M. D. H.; Cobden, P. L.; McEuen, N.; Chopra, A.; Zettl, A.; Thess, A. R.; Smalley, R. E. *Science* **1997**, *275*, 1922.
(4) Baughman, R. H.; Changxing, C.; Zakhidov, A. A.; Iqbal, Z.; Barisci, J. N.; Spinks, G. M.; Wallace, G. G.; Mazzoldi, A.; de Rossi, D.; Rinzler, A. G.; Jaschinski, O.; Roth, S.; Kertesz, M. *Science* **1999**, *284*, 1340.
(5) de Herr, W. A.; Bonard, J.-M.; Fauth, K.; Chatelain, A.; Forro, L.; Ugarte, D. *Adv. Mater.* **1997**, *9*, 87.
(6) Che, G.; Lakshmi, B. B.; Fisher, E. R.; Martin, C. R. *Nature* **1998**, *393*, 346.
(7) Ding, W.; Eitan, A.; Fisher, F. T.; Chen, X.; Dikin, D. A.; Andrews, R.; Brinson, L. C.; Schadler, L. S.; Ruoff, R. S. *Nano Lett.* **2003**, *3*, 1593.
(8) Gong, K.; Zhang, M.; Yan, Y.; Su, L.; Mao, L.; Xiong, S.; Chen, Y. *Anal. Chem.* **2004**, *76*, 6500.
(9) Pradhan, B. K.; Toba, T.; Kyotani, T.; Tomita, A. *Chem. Mater.* **1998**, *10*, 2510.
(10) Didenko, V. V.; Moore, V. C.; Baskin, D. S.; Smalley, R. E. *Nano Lett.* **2005**, *5*, 1563.
(11) Lee, W.; Wang, C. Y.; Shin, Y.-C. *Appl. Phys. Lett.* **2004**, *85*, 513.
(12) Baik, I.-S.; Lee, J.-Y.; Jeon, S.-Y.; An, K.-H.; Choi, J.; Lee S.-H.; Lee, Y.-H. *Proceedings of the 5th International Meeting on Information Display*; Korean Information Display Society, Seoul, July 19−23, 2005; p 415.
(13) Jeon, S. Y.; Park, K. A.; Baik, I.-S.; An, K. H.; Choi, J.; Lee, S. H.; Lee, Y. H. *Proceedings of the 12th International Display Workshops*; The Institute of Image Information and Television Engineers and Society for Information Display, Takamatsu, December 6−9, 2005; p 167.
(14) Lee, W.; Gau, J.-S.; Chen, H.-Y. *Appl. Phys. B* **2005**, *81*, 171.
(15) Huang, C.-Y.; Hu, C.-Y.; Pan, H.-C.; Lo, K.-Y. *Jpn. J. Appl. Phys.* **2005**, *44*, 8077.
(16) Baik, I.-S.; Lee, J. Y.; Jeon, S. Y.; An, K. H.; Choi, J. W.; Lee, S. H.; Lee, Y. H. *Appl. Phys. Lett.* **2005**, *87*, 263110.
(17) Lynch, M. D.; Patrick, D. L. *Nano Lett.* **2002**, *2*, 1197.
(18) Dierking, I.; Scalia, P.; Morales, P. *J. Appl. Phys.* **2005**, *97*, 044309.
(19) Jeon, S. Y.; Baik, I-S.; Lee, J. Y.; An, K. H.; Choi, J. W.; Lee, S. H.; Lee, Y. H. *Proceedings of the 8th European Conference on Liquid Crystals*; Organized by Società Italiana Cristalli Liquidi, Sesto (BZ), February 27−March 4, 2005; p 65.
(20) Baik, I.-S.; Jeon, S. Y.; Jeong, S. J.; Lee, S. H.; An, K. H.; Jeong, S. H.; Lee, Y. H. *J. Appl. Phys.* **2006**, *100*, 074306.
(21) The DMol^3 is a registered software product of Accelrys, Inc.
(22) Perdew, J. P.; Wang, Y. *Phys. Rev. B* **1992**, *45*, 13244.
(23) Perdew, J. P.; Wang, Y. *Phys. Rev. B* **1986**, *33*, 8800.
(24) (a) Esumi, K.; Ishigami, M. I.; Nakajima, A.; Sawada, K.; Honda, H. *Carbon* **1996**, *34*, 279. (b) Pan, H.; Feng, Y. P.; Lin, J. Y. *Phys. Rev. B* **2004**, *70*, 245425.
(25) De Gennes, P. G.; Prost, J. *The Physics of Liquid Crystals*, 2nd ed.; Clarendon Press, Oxford, 1993.
(26) Tasis, D.; Tagmatarchis, N.; Bianco, A.; Praton, M. *Chem. Rev.* **2006**, *106*, 1105.